

Cover Page



Universiteit Leiden



The handle <http://hdl.handle.net/1887/25491> holds various files of this Leiden University dissertation

**Author:** Vorst, Joost van der

**Title:** Near-infrared fluorescence-guided surgery : pre-clinical validation and clinical translation

**Issue Date:** 2014-05-01

# Chapter 3

## **Intraoperative fluorescence delineation of head and neck cancer with a fluorescent anti-epidermal growth factor receptor nanobody**

van Driel PB<sup>1</sup>, van der Vorst JR<sup>1</sup>, Verbeek FP, Oliveira S, Snoeks TJ, Keereweer S,  
Chan B, Boonstra MC, Frangioni JV, van Bergen en Henegouwen PM,  
Vahrmeijer AL, Lowik CW

*<sup>1</sup>Both authors contributed equally to this work and share first-authorship*

*Int J Cancer. 2013 Nov 13*

## **ABSTRACT:**

### **Background**

Intraoperative near-infrared (NIR) fluorescence imaging is a technology with high potential to provide the surgeon with real-time visualization of tumors during surgery. This study explores the feasibility for clinical translation of an epidermal growth factor receptor (EGFR) targeting nanobody for intraoperative imaging and resection of orthotopic tongue tumors and cervical lymph node metastases.

### **Material and Methods**

The anti-EGFR nanobody 7D12 and the negative control nanobody R2 were conjugated to the NIR fluorophore IRDye800CW (7D12-800CW and R2-800CW). Orthotopic tongue tumors were induced in nude mice using the OSC-19-luc2-cGFP cell line. Tumor bearing mice were injected with 25 $\mu$ g 7D12-800CW, R2-800CW or 11 $\mu$ g 800CW. Subsequently, other mice were injected with 50  $\mu$ g or 75  $\mu$ g of 7D12-800CW. The FLARE imaging system and the IVIS spectrum were used to identify, delineate and resect the primary tumor and cervical lymph node metastases.

### **Results**

All tumors could be clearly identified using 7D12-800CW. A significantly higher tumor-to-background ratio (TBR) was observed in mice injected with 7D12-800CW compared to mice injected with R2-800CW and 800CW. The highest average TBR ( $2.00 \pm 0.34$  and  $2.72 \pm 0.17$  for FLARE and IVIS spectrum, respectively) was observed 24 hours after administration of the EGFR-specific nanobody. After injection of 75  $\mu$ g 7D12-800CW cervical lymph node metastases could be clearly detected. Orthotopic tongue tumors and cervical lymph node metastases in a mouse model were clearly identified intraoperatively using a recently developed fluorescent EGFR targeting nanobody.

### **Conclusion**

Translation of this approach to the clinic would potentially improve the rate of radical surgical resections.

## INTRODUCTION

In oncology, a range of noninvasive imaging modalities, including X-ray, ultrasonography, computed tomography (CT) and magnetic resonance imaging (MRI), enable early detection, staging, and treatment evaluation of cancer. However, in most cases surgeons still discriminate healthy tissue from cancerous tissue by means of visual inspection and palpation during surgery. Given the fact that adequate tumor free margins are of paramount importance for patient prognosis and outcome, and that irradical resections still frequently occur, novel imaging modalities are needed. Despite the primary objective of achieving macroscopic clearance of 1 cm in the surgical management of oropharyngeal or oral squamous cell carcinoma (OSCC), the presence of tumor positive margins has been reported in 16% of patients.<sup>1</sup> Numerous reports have indicated that involved margins imply deteriorated prognoses.<sup>2</sup> On the other hand, applying wider surgical margins will result in functional impairment in most cases.<sup>3,4</sup> Therefore, clearer delineation of the tumor during surgery may improve the number of radical resections, thus increasing patients' survival rates while maintaining postoperative functionality.

Near-infrared (NIR) fluorescence imaging is a novel imaging technique that provides the surgeon with real-time visualization of tumors during surgery.<sup>5-7</sup> In the NIR region (650 – 800 nm), less absorption of light by tissue components allows much deeper penetration of light. Furthermore, lower fluorescence from endogenous fluorophores decreases the non-specific background signal. As the human eye is not sensitive to NIR fluorescent light, a specific NIR fluorescence imaging system is needed to visualize the fluorescence signal. At the same time, since NIR light is invisible to the human eye, it will not alter the surgical field.<sup>8</sup>

One of the main challenges in intraoperative fluorescence imaging lies in the development, validation and clinical introduction of a tumor specific agent. Being widely overexpressed in OSCC, the epidermal growth factor receptor (EGFR) serves as an interesting target for intraoperative fluorescence imaging.<sup>9,10</sup> The EGFR is a transmembrane glycoprotein that is involved in DNA synthesis and cell proliferation. Overexpression contributes to oncogenesis by proliferation, dedifferentiation, inhibition of apoptosis, invasiveness and lack of adhesion dependence.<sup>11</sup> Furthermore, EGFR overexpression is often associated with a poor prognosis for patients with OSCC.<sup>12</sup>

For tumor targeting using molecular imaging techniques, antibodies are promising as they can be raised specifically against practically any molecular

target. Nevertheless, due to their large hydrodynamic diameter, intact antibodies accumulate in the liver. Moreover, long half-life in the bloodstream and slow blood clearance via the liver results in high contrast images only several days after injection. A very appealing alternative is the use of nanobodies.<sup>13</sup> Nanobodies are the smallest functional antigen-binding fragments derived from naturally-occurring heavy-chain only antibodies.<sup>14</sup> They show very specific binding to their targets and their size of approximately 15 kDa ensures efficient distribution and tissue penetration, as well as rapid clearance from the body.<sup>15-17</sup>

This study assesses the feasibility of intraoperative fluorescence delineation of orthotopic OSCC and microscopic lymph node metastases, using an anti-EGFR nanobody and a clinically available fluorescence camera system. For this, the anti-EGFR nanobody 7D12 was conjugated to the NIR fluorophore IRDye800CW.<sup>18</sup>, as previously described by Oliveira et al.<sup>17</sup>. Tumor accumulation and specificity of 7D12-800CW was compared to the negative control nanobody R2-800CW and to 800CW alone.

## **MATERIAL and METHODS**

### **Cell lines and culture**

Two human cell lines were used. For the animal studies, the metastatic oral squamous cell carcinoma (OSCC) line OSC-19 was used. The OSC19 cell line was established in Japan with cells from a patient with a well-differentiated squamous cell carcinoma of the tongue that metastasized to a cervical lymph node.<sup>19</sup> Luc2 luciferase from pGL4.10 plasmid (Promega, Madison, WI, USA) was cloned into the multiple cloning site (MCS) of the lentiviral vector pCDH-EF1-MCS-T2A-copGFP (Biacat, Heidelberg, Germany) using specific primers with the corresponding restriction sites. OSC-19 cells were transduced by self-inactivating lentiviral vectors as previously described<sup>20</sup> and positive cell clones selected by limit dilution to create a stable luciferase 2 (luc2) and green fluorescent protein (GFP) expressing OSC-19-Luc2-copGFP cell line. The cells were grown *in vitro* in Dulbecco's Modified Eagle's Medium (DMEM, Invitrogen, Carlsbad, CA, USA) containing 4.5 g D-Glucose/L, 110 mg sodium pyruvate/L, 580 mg L-glutamine/L supplemented with 10% fetal bovine serum (FCS; Lonza, Basel, Swiss), 100 IU/mL penicillin, 100 µg/mL streptomycin (Invitrogen), 1x Minimal Essential Medium (MEM) Non-Essential Amino Acids solution and 1x MEM vitamin solution (Invitrogen). The human colorectal cancer cell line SW620 was used as an EGFR

negative control. This cell line was cultured in Leibovitz's L-15 medium (Invitrogen) containing 300 mg L-glutamine/L supplemented with 10% FetalClone II (Hyclone, Logan, UT, USA) 100 IU/mL penicillin, 100 µg/mL streptomycin (Invitrogen) and 20 mM HEPES (Invitrogen). All cell lines were grown in a humidified incubator at 37°C and 5% CO<sub>2</sub>. Cells were regularly checked for *Mycoplasma* infection by PCR.

### **Nanobodies and Conjugation to IRDye800CW**

Two nanobodies were used: 7D12 and R2. The EGFR specific nanobody 7D12 binds to the ectodomain of the EGFR.<sup>18,21</sup> EGFR specificity of 7D12-800CW *in vitro* and *in vivo* was reported earlier.<sup>17</sup> The nanobody R2 was used as a non-EGFR specific control.<sup>22,23</sup> Both nanobodies have a molecular weight of approximately 15 kDa and show similar *in vivo* biodistribution.<sup>17,18,24</sup> The generation of the nanobodies 7D12 and R2 was described previously.<sup>18,23</sup> Induction of protein expression and purification of nanobodies from the periplasmic space of *Escherichia coli* were performed as described by Roovers et al.<sup>25</sup> Conjugation of both nanobodies to the NIR fluorophore IRDye800CW was performed as described by Oliveira et al.<sup>17</sup> Briefly, the IRDye800CW N-hydroxysuccinimide ester (LI-COR, Lincoln, NE, USA) was added to the protein in a 4-fold molar excess and was incubated for two hours at room temperature. Removal of the unconjugated fluorophore was accomplished by using two Zeba Spin Desalting columns (Thermo Fisher Scientific, Perbio Science Nederland B.B., Ettenleur, the Netherlands) per protein in two sequential steps. The fluorescent nanobodies, i.e. 7D12-800CW and R2-800CW, were characterized as previously described<sup>17</sup>, namely for their conjugation efficiency and these parameters were in agreement with previous values, i.e. 0.5 and 1.1, respectively.

### **EGFR expression**

OSC-19 and SW620 cells were cultured until subconfluence. Cells were detached with trypsin and adjusted at  $1 \times 10^5$  cells/tube in ice cold PBS, 10% FCS (Lonza, Basel, Swiss) and 1% sodium azide. The anti-EGFR monoclonal antibody sc-120 alexa fluor 647 (Santa Cruz biotechnology, Santa Cruz, CA, USA) or non-specific normal mouse IgG<sub>2a</sub> alexa fluor 647 (Santa Cruz) were added and cells were incubated in the dark on ice for 30 minutes. After incubation, cells were washed three times in ice cold PBS and resuspended in ice cold PBS, containing 10% FCS (Lonza) and 1% sodium azide. Flow cytometry of alexa fluor 647 labeled cells was performed using the BD LSR II (BD biosciences, San Jose, CA, USA). EGFR expression was estimated as the geometric mean of fluorescence intensity measured in 10.000 viable cells. The experiment was performed in duplicate.

### **Binding study**

A binding assay was performed to confirm the specificity of the EGFR binding of 7D12-800CW. A black 96-well plate (Greiner bio-one, Frickenhausen, Deutschland) was used in which 20.000 OSC-19-luc2-cGFP and SW620 cells were seeded per well. After one day, cells were washed with binding medium (DMEM supplemented with 25 mM Hepes and 1% BSA, at pH 7.2). 7D12-800CW (7D12), R2-800CW (R2) and IRDye800CW carboxylate (800CW, LI-COR, Lincoln, NE, USA) were added in triplicate in a concentration range of 0 to 50 nM. R2-800CW and IRDye800CW carboxylate were used as negative controls. The cells were incubated for 2 hours in the dark on a rocker at 4°C and afterwards washed two times with binding medium. Bound proteins were directly observed with the Odyssey scanner (LI-COR), scanning at 800 nm. Directly after these measurements cells were fixed with 4% paraformaldehyde and incubated with TO-PRO-3 (Invitrogen) at 1:5000 for 15 minutes. Again cells were washed twice and the plate was imaged using the 700nm channel of the Odyssey (LI-COR) to detect TO-PRO3 fluorescence. Nucleus staining was performed to correct the fluorescence signal for the amount of cells enabling direct comparison of fluorescence signal of both cell lines.

### **Fluorescence imaging systems**

Real-time fluorescence imaging of primary tumor and lymph node metastases was performed using the FLARE imaging system.<sup>26</sup> Briefly, This imaging system consists of three wavelength-isolated light sources: a 400-650 nm light source generating 40.000 lux (white light), a 656-678 nm light source generating 4 mW/cm<sup>2</sup> (700 nm) and a 745 – 779 nm light source generating 14 mW/cm<sup>2</sup> (800 nm). The imaging head, attached to a flexible gooseneck arm, enables real-time image acquisition from all three cameras. Color, NIR fluorescence and pseudo-colored (lime green) merged images are displayed in real time. Next to the FLARE imaging system, the IVIS spectrum (Caliper Life Science, Hopkinton, MA, USA) was used to visualize primary tumors and metastases. Data analysis of FLARE and IVIS spectrum data was performed using image J and the *Living Image* software from xenogen version 3.2 (Caliper LS) respectively. Multiple regions of interest (ROI) were drawn in the tumor and in adjacent normal tissue of the tongue and divided by each other to calculate TBRs.

### Animal model

Nude Balb/c female mice (Charles River laboratories, l'Arbresle, France), aged 4 – 6 weeks, were housed in individually ventilated cages and provided with food and sterilized water ad libitum. Animal experiments were approved by the local animal welfare committee of the Leiden University Medical Center.

Orthotopic tongue tumors were submucosally induced in the tip of the tongue through injection of 40.000 OSC-19-luc2-cGFP cells, diluted in 20  $\mu$ L phosphate-buffered saline (PBS). Mice body weight was monitored twice a week and tumor growth was monitored twice a week by bioluminescence (BLI) measurements and visual inspection of the tongue. BLI signal, being the most sensitive imaging method for the detection of tumor cells<sup>27</sup>, served as an *in vivo* control for the tumor specific fluorescence of the nanobodies. Imaging procedures were performed under isoflurane gas anesthesia. Weight measurements and tongue inspections were performed to monitor general health during the experiments. Mice were sacrificed by injection of high doses ketamine/xylazine.

### Fluorescence measurements

Twenty days after injection of tumor cells, mice (n = 9) were randomly divided into three groups and received a systemic injection of 25  $\mu$ g 7D12-800CW (1.6 nmol, 64 nmol/kg), 25  $\mu$ g R2-800CW (1.5 nmol, 60 nmol/kg) or 11  $\mu$ g 800CW carboxylate (1 nmol, 40 nmol/kg, LI-COR). For the two nanobodies, a previous study reported 25  $\mu$ g to be the optimal dose.<sup>17</sup> Fluorescent images were acquired at 0.5, 1, 2, 4, 8, 24 and 48 hours after injection.

For the detection of microscopic cervical lymph node metastases two additional concentrations of 50 and 75  $\mu$ g 7D12-800CW were injected (n = 4). Mice were sacrificed at 24 hours after injection and overlying skin of the cervical region was removed for gross examination. Whole-body fluorescence imaging was performed and the tongue and cervical lymph nodes were subsequently resected.

### Histology and fluorescence microscopy

After *ex vivo* fluorescent measurements, the resected tongues were cut in two. One half was frozen on dry ice, the other half fixed in 4% formalin overnight and embedded in paraffin blocks. Cervical lymph nodes on both sides were resected. The left lymph node was frozen on dry ice, the right lymph node paraffin embedded and fixed in 4% formalin overnight. Tissue was sectioned at 10  $\mu$ m and imaged using the Odyssey (LI-COR). All images were acquired using the same settings but

the images (i.e. brightness and contrast) of the control probes were altered to show any fluorescence and emphasize the difference in localization between specific and non-specific probes. To confirm the presence of tumor cells, fluorescence microscopy (Nikon eclipse e800, Nikon, Amsterdam, the Netherlands) of the GFP fluorescence signal emitted by OSC-19-luc2-cGFP cells was performed on frozen tissue slices. Histologic sections were stained with standard hematoxylin-eosin stain (HE). As expected, fluorescence of GFP could not be detected in paraffin embedded sections. Therefore, the presence of smaller cervical lymph node metastases in paraffin sections was confirmed by staining the cervical lymph node sections with anti-human wide-spectrum cytokeratin staining (Abcam inc., Cambridge, MA, USA).

### **Statistical analysis**

For statistical analysis, SPSS statistical software package (Version 16.0, Chicago, IL) was used. TBR's were calculated by dividing the fluorescent signal of the tumor by fluorescent signal of surrounding tissue. TBR was reported in mean and standard deviation. To compare TBR between dose groups and time points, and to assess the relation between dose and time, a mixed model analysis was used. When a significant difference was detected, a one-way ANOVA was used to post-test for differences between separate dose groups and/or time points. The one-way ANOVA was corrected using the Bonferroni correction.  $P < 0.05$  was considered significant. Differences between the FLARE and IVIS imaging systems were tested with an unpaired T-test.

## RESULTS

### In vitro results

The specificity of the EGFR targeting nanobody for the squamous cell carcinoma of the tongue, that metastasizes to cervical lymph nodes, was first validated *in vitro*. For that purpose, we started with the evaluation of the EGFR expression in the OSC-19-luc2-cGFP cell line. Direct staining of the cell surface epitope of the EGFR of OSC-19-luc2-cGFP cells caused an increase in fluorescence intensity, as shown by a shift to the right through flow cytometry analyses, compared to the non-specific antibody (Fig 1A). Next, as a control to the EGFR overexpressing OSC-19-luc2-cGFP cell line, we assessed the EGFR expression in the human colon carcinoma cell line SW620, a cell line that has no overexpression of the EGFR. In contrast to OSC-19-luc2-cGFP, the FACS data of this cell line revealed no increase in fluorescence intensity, thus confirming the absence of EGFR expression in the SW620 cell line (Fig 1B).

Both these cell lines were employed to confirm the specificity of the EGFR targeting nanobody 7D12-800CW, which was compared to the non-EGFR specific nanobody R2-800CW and to 800CW alone. The IRDye800CW-conjugated probes were produced and characterized as described by Oliveira et al.<sup>17</sup> Consistently, after purification of the conjugates through removal of unconjugated fluorophores, a small percentage of the 800CW unconjugated fluorophore (less than 7.5 % of the 800CW conjugated fraction) was still present (data not shown) and the fluorophore to protein molar ratio of 7D12-800CW and R2-800CW after random conjugation was 0.5 and 1.1 respectively.

The cell assay, performed at 4°C to prevent internalization and investigate binding only, clearly demonstrated an EGFR specific binding of 7D12-800CW in OSC-19-luc2-cGFP cells that proved to be concentration dependent (Fig 1C). With R2-800CW and 800CW, although slightly concentration dependent, significantly less fluorescence intensity was observed (Fig 1C). In the EGFR negative cell line no significant differences in fluorescence intensity between 7D12-800CW and R2-800CW were observed. Altogether, these results confirm the specificity of 7D12-800CW for binding to EGFR and show that both the negative control R2-800CW and the 800CW alone do not associate with these cells (Fig 1C and 1D).

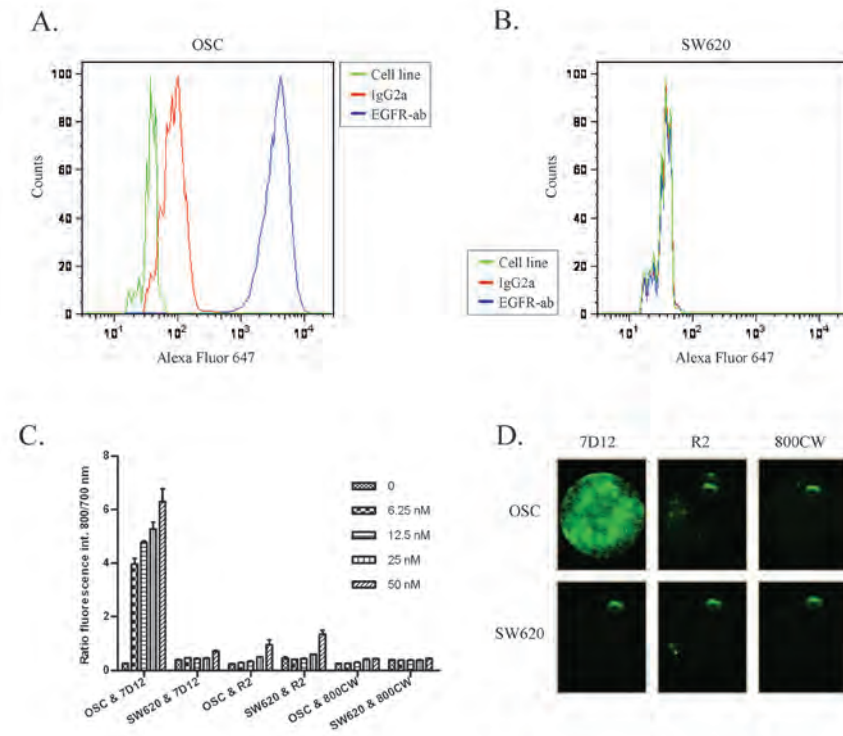


**Figure 1 – EGFR expression and binding assay:** Flow cytometry was performed using OSC-19-luc2-cGFP and SW620 without antibody (green), with an EGFR specific antibody conjugated to alexa fluor 647 (blue) and with an isotype control normal mouse IgG2a conjugated to alexa fluor 647 (red). 7D12-800CW binds to human epidermal growth factor receptor expressed on OSC19-luc2-cGFP cells.

A. The EGFR is highly expressed on the surface of OSC-19-luc2-cGFP cells.

B. No expression of EGFR was found on the surface of SW620 cells.

C. The human EGFR expressing OSC cells and EGFR negative SW620 cells were incubated with different concentrations of 7D12-800CW, R2-800CW and 800CW. The ratio of the fluorophore bound protein and the fluorescence intensity of TO-PRO-3 was plotted to correct for the amount of cells. Every concentration was performed in triplicate. Error bars indicate the standard deviation.

D. Images were acquired with the Odyssey Scanner (LICOR). OSC and SW620 cells were incubated with 50 nM 7D12, R2 and 800CW. OSC = OSC-19-luc2-cGFP.

## Animal model

Within three weeks after orthotopic inoculation of OSC-19-luc2-cGFP cells in the tip of the tongue, all mice developed a primary tongue tumor and cervical lymph node metastases (a typical example is shown in Fig 2A), observed during regular visual inspection and confirmed by the increase in mean bioluminescence signal (Fig 2B)

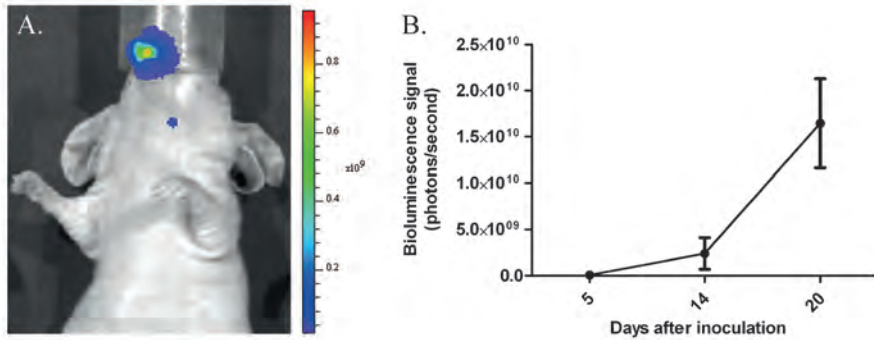


**Figure 2 - Tumor growth followed by imaging bioluminescence:**

A. Bioluminescent image after injection of OSC-19-luc2-cGFP cells. Primary tongue tumor and lymph node metastasis are shown.

B. Increase of tumor growth (measured in bioluminescence signal) as a function of time.

### In vivo NIR Fluorescence Imaging of primary tumors

Three weeks after tumor cell inoculation, mice were injected intravenously with 25  $\mu\text{g}$  of 7D12-800CW, R2-800CW or 11  $\mu\text{g}$  800CW (for equivalent fluorescence to 7D12-800CW). To assess the feasibility of a possible clinical translation, fluorescence images were taken with both the preclinical, highly sensitive IVIS spectrum camera as well as with the FLARE intraoperative imaging system. As demonstrated in Figure 3A, all tumors of the animals that were injected with 7D12-800CW could be clearly identified through NIR fluorescence using both imaging modalities. No adequate tumor-to-background ratios were observed in the control mice injected with R2-800CW or 800CW (Fig 3B), which is in agreement with the results obtained in vitro (Fig 1). Using the IVIS imaging system, a mixed model showed significant differences in TBRs between three study groups and between time points ( $p < 0.0001$  and  $p < 0.0001$ , respectively) (Fig 4A). Post-testing using a one-way ANOVA showed significant differences between the 7D12-800CW and the R2-800CW ( $p < 0.0001$ ) study groups and between the 7D12-800CW and 800CW ( $p < 0.0001$ ) study groups. No significant difference was found between R2-800CW and 800CW ( $p > 0.999$ ). The highest TBR ( $2.72 \pm 0.17$ ) was measured at 24 hours after administration of 7D12-800CW. Using the FLARE imaging system, a mixed model showed significant differences in TBRs between the three study groups and between time points ( $p = 0.041$  and  $p < 0.0001$ , respectively) (Fig 4B). Post-testing using a one-way ANOVA showed significant differences between the 7D12-800CW and the R2-800CW study groups ( $p = 0.05$ ) and between the 7D12-800CW and 800CW study groups ( $p = 0.002$ ). No significant difference was found between R2-800CW and

800CW ( $p = 0.77$ ). The highest TBR ( $2.00 \pm 0.34$ ) was measured at 24 hours after administration of 7D12-800CW. The highest TBR measured with the IVIS imaging system was significantly higher compared to the highest TBR measured with the FLARE imaging system ( $p = 0.03$ ).

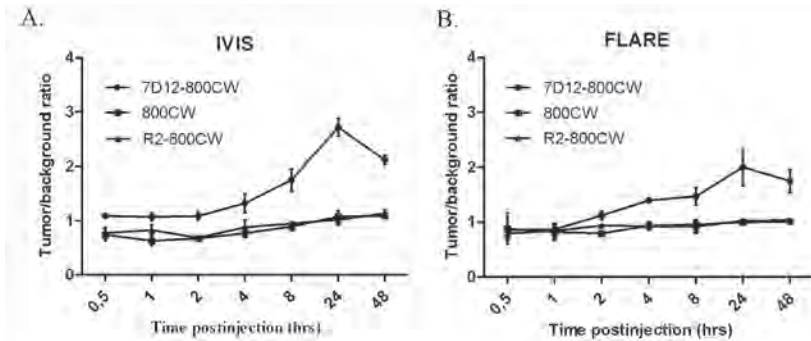


**Figure 4 - Intraoperative tumor to background ratios over time:** The tumor to background ratio of 7D12-800CW is significantly higher compared to those of R2-800CW and 800CW. Tumor to background ratios were calculated from 0.5 hours to 48 hours after injection. Error bars indicate the standard deviation. Tumor to background ratios were plotted for the IVIS-Spectrum (A) and the FLARE imaging system (B).

### **Ex vivo fluorescence imaging and histology of primary tumors**

In cryo sections, fluorescent imaging of the GFP that was transduced in the OSC-19 cells confirmed the presence of tumor cells in the tongue (Fig 5). After fluorescent imaging (GFP and NIR fluorescence), sections were stained with HE. Even sub-millimeter islands of tumor cells, confirmed with GFP fluorescence, co-localized with the fluorescence of 7D12-800CW, as measured with the Odyssey Scanner (Fig 5). No co-localization was observed in the tongue specimens of mice injected with R2-800CW or 800CW, which is in agreement with our observations *in vivo* (Fig 3B).

### **In vivo and ex vivo fluorescence imaging and histology of cervical lymph nodes**

In contrast to the primary tumor, microscopic cervical lymph node metastases were not grossly visible. In fact, a dose of 75  $\mu\text{g}$  of 7D12-800CW only gave a weak fluorescence signal through the skin using the IVIS, but, importantly, a strong fluorescence with both imaging systems could be detected when the skin was removed (Fig 6). This highlights the potential of this imaging modality in the intraoperative context.

During *ex vivo* imaging, the fluorescence of GFP that was transfected in the OSC-19-luc2-cGFP cells confirmed the presence of cervical lymph node metastases in the tissue specimen and could be colocalized to the fluorescent signal of 7D12-800CW. As expected, due to bleaching and the washing steps, no GFP fluorescence was found in the paraffin sections of the cervical lymph nodes. Nevertheless,

immunohistochemical analysis, using a wide spectrum anti-cytokeratin staining, confirmed the presence of tumor cells. As shown in Figure 6, the fluorescence signal of 7D12-800CW co-localizes with the tumor cells in the cervical lymph node.

## DISCUSSION

In the present study, the EGFR targeting nanobody conjugated to 800CW was used to delineate orthotopic OSCC tumor margins during surgery. After 2 hours post injection tumors could already be clearly delineated. The highest TBR was obtained 24 hours after injection. Furthermore, a significant difference in TBR was observed between mice injected with 7D12-800CW, and mice injected with the control nanobodyR2-800CW or with 800CW alone.

NIR fluorescent optical imaging is an imaging technique with high potential to obtain real-time information about the presence, location and dimensions of tumor tissue so that adequate tumor free margins can be obtained after resection.<sup>28-30</sup> Although the first clinical trial has recently been performed<sup>29</sup>, it remains challenging to find a suitable fluorescent probe which can be detected with a sensitive NIR-fluorescent imaging system.

The first challenge to NIR fluorescence imaging is the optimal fluorescent probe. An ideal fluorescent probe should distribute well, have a high affinity towards its target and a fast clearance from the bloodstream, to allow efficient accumulation at the tumor and rapid acquisition of images with high contrast. Furthermore, no accumulation in the liver is desirable and the ability to adequately penetrate the tissue of interest is of great importance. The EGFR serves as a very interesting target in head and neck cancer as the majority of these cancers overexpress this receptor.<sup>10,31</sup> In a previous study we used recombinant human EGFR ligands conjugated to 800CW to target head and neck tumors.<sup>32</sup> Although efficient in targeting head and neck tumors, recombinant human EGFR ligands can potentially activate this receptor, which promotes its malignant phenotype. In other studies, cetuximab conjugated to Cy5.5 and panitumumab conjugated to 800CW are used to image head and neck tumors.<sup>9,33</sup> Conventional antibodies, however, show slower blood clearance (up to several days), higher accumulation in the liver and limited tumor penetration compared to nanobodies.<sup>17</sup> For these reasons, we have selected a nanobody as our probe for this study.

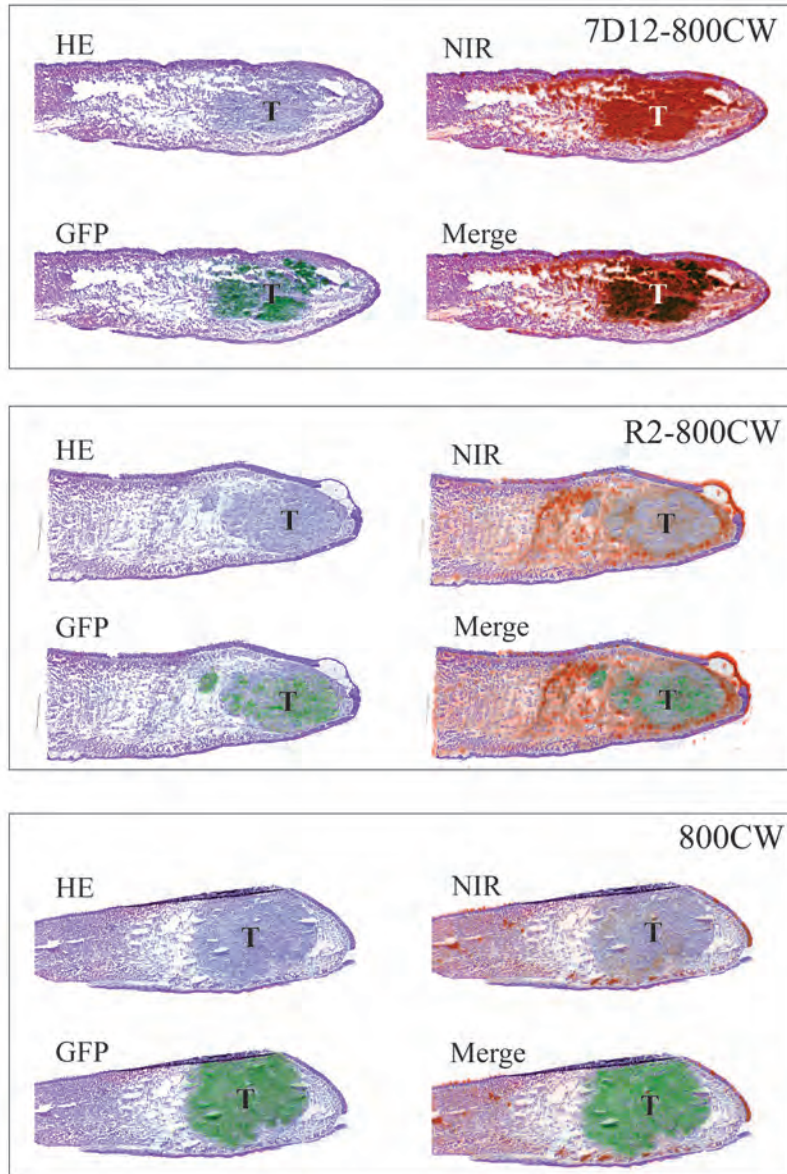


**Figure 5 - Histology and fluorescence imaging of orthotopic primary tongue tumors:** Shown are hematoxylin and eosin (HE) stainings, HE and GFP fluorescence overlays, HE and NIR fluorescence overlays and HE, NIR and GFP fluorescence overlays. In the 7D12-800CW tissue specimen, a clear overlap between NIR and GFP (indicating tumor cells) fluorescence was observed. In the R2-800CW and 800CW specimens, no overlap between NIR and GFP fluorescence was observed. Brightness and contrast of the images of R2-800CW and 800CW was altered to show fluorescence and emphasize the localization in tissue.

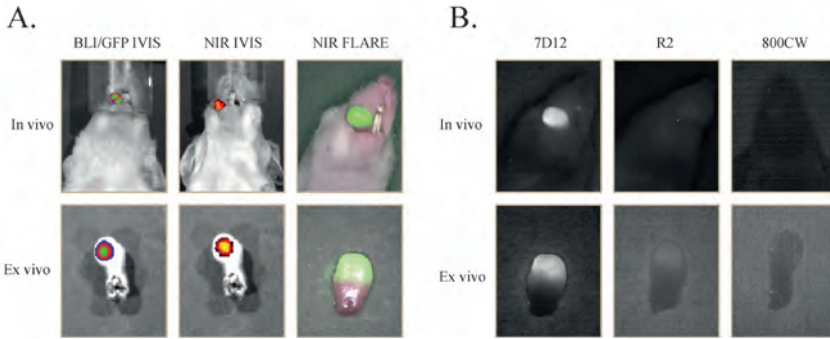


**Figure 3 – Multimodal *in vivo* and *ex vivo* imaging of an orthotopic tongue tumor:** 7D12 is specifically taken up in the oral squamous cell carcinoma of the tongue. Mice bearing OSC-19-luc2-cGFP human xenografts were intravenously injected with 25µg of 7D12, R2 and 800CW. After 24 hours fluorescent images were obtained with the IVIS spectrum and the intraoperative camera system (FLARE).

A. *In vivo*: bioluminescence brightfield merge image (left), NIR fluorescence brightfield merge IVIS image of 7D12-800CW (middle) and NIR fluorescence color merge FLARE image (right) *Ex vivo*: GFP brightfield merge image (left), NIR fluorescence brightfield merge IVIS image of 7D12-800CW (middle) and NIR fluorescence color merge FLARE image (right)

B. *In vivo*: Fluorescent imaging of a tongue tumor 24 hours after administration of 7D12-800CW (left), R2-800CW (middle) and 800CW (right). *Ex vivo*: Fluorescent imaging of a tongue tumor 24 hours after administration of 7D12-800CW (left), R2-800CW (middle) and 800CW (right). Images were obtained with the intraoperative camera system (FLARE)

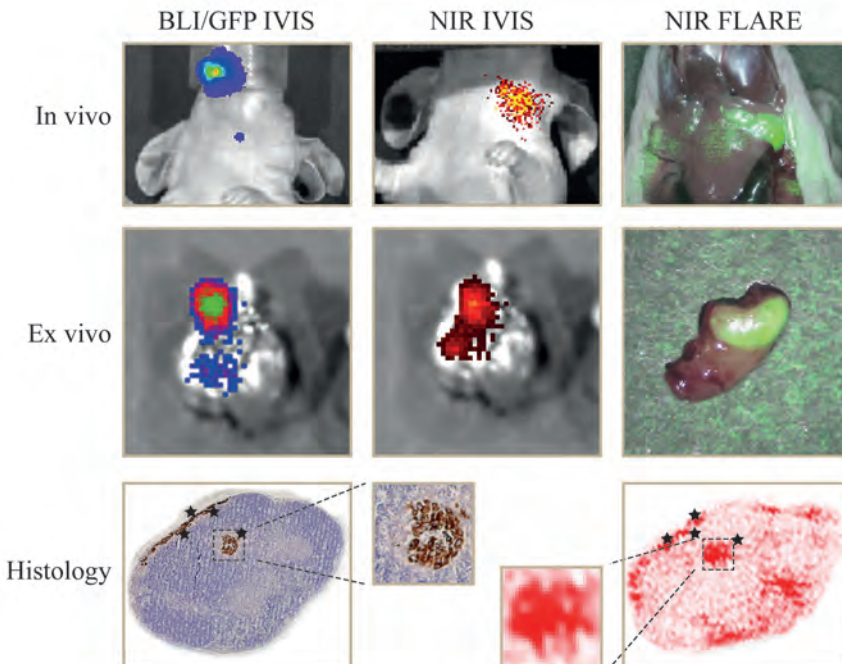


**Figure 6 – *In vivo*, *ex vivo* and histological fluorescence imaging of cervical lymph nodes:**

*In vivo*: bioluminescence brightfield merge image (left), NIR fluorescence brightfield merge IVIS image of 7D12-800CW (middle) and NIR fluorescence color merge FLARE image (right)

*Ex vivo:* GFP brightfield merge image (left), NIR fluorescence brightfield merge IVIS image of 7D12-800CW (middle) and NIR fluorescence color merge FLARE image (right)

*Histology:* Shown are a hematoxylin and eosin (HE) staining combined with a cytokeratin staining (left) and NIR fluorescence image (right) of a cervical lymph node of a mice injected with 7D12-800CW. A clear overlap between NIR fluorescence and the brown cytokeratin staining (indicating tumor cells) was observed.

Next to the ideal probe, the extent to which a tumor can be visualized during surgery is highly depending on the NIR fluorescent imaging system. Gioux et al.<sup>34</sup> have reviewed the technical requirements for an intraoperative imaging system. To assess the feasibility of translating our results into clinical experiments, we used the clinically available FLARE™ imaging system. This system is able to adequately detect microscopic disease intraoperatively and has proven its clinical use in over 25 clinical trials.<sup>26,35</sup> Using the IVIS spectrum we were able to measure bioluminescence and confirm the presence of tumor cells *ex vivo*, by imaging GFP fluorescence of the transfected OSC-19-luc2-cGFP cells. Furthermore, fluorescence measurements obtained with the IVIS spectrum, i.e. a closed ('black box') preclinical imaging system, were compared with the measurements of the clinically available FLARE™ imaging system. This comparison showed a significant difference in TBR favoring the IVIS spectrum on the optimal imaging time point (24hr post injection). This difference can be explained by the fact that the IVIS spectrum is, in contrary to the FLARE imaging system, a 'black box' imager with less daylight interfering and subsequently less background fluorescence. However, since this device obviously cannot be used intraoperatively, the FLARE imaging system is an adequate alternative as the average TBR was over 2.

In previous studies, we used the EGFR targeted nanobody 7D12 conjugated to 800CW to image subcutaneous A431 tumor xenografts, which have high EGFR expression.<sup>17</sup> Undoubtedly, the host microenvironment has great influence on tumor biology that affects parameters such as angiogenesis, growth, invasion, metastasis and lymphangiogenesis. Therefore, an orthotopic model is clinically a more relevant model with great importance to assess the ability of a probe for fluorescence delineation of tumors and its possible translation to the clinic. In this study, we successfully tested the potentiality of intraoperative fluorescence delineation of orthotopic OSCC and microscopic lymph node metastases using a clinically available fluorescence imaging system. Based on these results we conclude that clinical translation of 7D12-800CW may be possible, using the FLARE imaging system in the intraoperative set-up.

A sufficient TBR is required to distinguish tumor from normal tissue<sup>30</sup> The

small molecular weight of 7D12 allows fast detection of the tumor due to rapid distribution and fast clearance of unbound molecules. Oliveira et al.<sup>17</sup> reported tumor detection from 30 minutes after injection onwards. In the present study, using both the FLARE and IVIS spectrum, the tumor could be sufficiently detected 2 hours post injection. The use of an orthotopic model in the tongue that differs in angiogenesis, lymphangiogenesis and interstitial pressure from a subcutaneous A431 tumor, could perhaps explain these variations. Nevertheless, the highest average tumor to background ratio (2.72 IVIS spectrum vs 2.0 FLARE) was obtained 24 hours after injection, which is in agreement with what was previously reported in the subcutaneous tumor model.<sup>17</sup> Although nanobodies distribute and bind to their targets very rapidly, the background signal is relatively high during the first hours. Monovalent nanobodies are not efficiently internalized and therefore bound nanobody can un-bind over a certain period of time.<sup>36</sup> The 7D12-800CW washout from normal tissue occurs faster than the release from its receptor in the tumor. As a result the TBR will increase over time until an optimal TBR is reached. After that, release of nanobody from its receptor will result in a decrease in TBR. A decreased TBR in our study was seen after 48 hours.

Cryosections of the tongue confirmed the tumor specific fluorescence by colocalization of the fluorescent signal of 7D12-800CW and the fluorescence of the GFP transfected OSC-19 cells. In the cryosections of mice injected with R2-800CW some fluorescence was detected, but there was no colocalization of NIR and GFP fluorescence. R2-800CW fluorescence mainly originated from the area surrounding the tumor. A possible explanation for the non-EGFR specific presence of R2-800CW could be the enhanced permeability and retention that is seen in many tumors.<sup>37</sup> Fluorescence could not be detected in the cryo sections of tongues of mice injected with 800CW alone.

When translating 7D12-800CW to the clinic, the specific binding of the nanobody to human EGFR could result in higher background fluorescence and therefore lower contrast. Importantly, Oliveira et al.<sup>17</sup> demonstrated the ability of 7D12-800CW to distinguish between different expression levels of EGFR *in vitro*. This implies that 7D12 could differentiate tumor tissue with high EGFR expression from normal tissue without overexpression of EGFR.

The prognosis of patients with head and neck cancer is largely dependent on lymph node involvement.<sup>38,39</sup> A sentinel lymph node (SLN) procedure could prevent elective neck dissections that are frequently performed for adequate staging and local control. Furthermore, despite the analysis by a trained pathologist, (micro)

metastases and occult tumor cells in lymph nodes can be missed by standard histopathological examination. Limited examination of one lymph node could increase the accuracy of staging in head and neck cancer. Recently van der Vorst et al.<sup>40</sup> demonstrated the feasibility to detect draining lymph nodes in head and neck cancers using the nonspecific fluorescent tracer ICG:HSA. The fluorescent tracer however, quickly migrated to lymph nodes beyond the SLN. This present study demonstrates the feasibility of specific targeting of cervical lymph node metastases. A dose of 75 µg of 7D12-800CW clearly allowed delineation of the primary tumor and identification of the cervical lymph node metastases after removal of the skin. Histology showed clear co-localization of the NIR fluorescence of 7D12-800CW and the cytokeratin staining, that confirmed the presence of tumor cells. Compared to the primary tumor however, an increase of nonspecific background signal was observed. Also, the smaller the tumor or metastases, the lower the fluorescent signal. Furthermore, the influence of optical properties on the light propagation through tissue can result in a blurred delineation of smaller tumors. Altogether, these aspects rendered visualization of the metastases slightly difficult, which was significantly improved by removal of the skin. Further research is needed to explore which is the minimum size of lymph node metastases that can be detected using 7D12-800CW. Intraoperative detection of lymph node metastases would be a better alternative to the non-specific SLN procedure. First, the efficiency of an intraoperative histopathological diagnosis on fresh-frozen sections could be increased by examination of the fluorescence positive lymph node. Eventually, the procedure might even prevent intraoperative pathologic analysis of fresh-frozen tissue sections.

In conclusion, the present study reports a recently developed fluorescent EGFR targeting nanobody, which clearly allowed the identification of orthotopic tongue tumors and cervical lymph node metastases in a mouse model. These results highlight the potential of this nanobody for clinical translation in the context of surgical management of oropharyngeal or OSCC.

## REFERENCES

1. McMahon J, O'Brien CJ, Pathak I et al. Influence of condition of surgical margins on local recurrence and disease-specific survival in oral and oropharyngeal cancer. *Br J Oral Maxillofac Surg* 2003; 41:224-231.
2. Iseli TA, Lin MJ, Tsui A et al. Are wider surgical margins needed for early oral tongue cancer? *J Laryngol Otol* 2012; 126:289-294.
3. Looser KG, Shah JP, Strong EW. The significance of "positive" margins in surgically resected epidermoid carcinomas. *Head Neck Surg* 1978; 1:107-111.
4. Loree TR, Strong EW. Significance of positive margins in oral cavity squamous carcinoma. *Am J Surg* 1990; 160:410-414.
5. Weissleder R, Pittet MJ. Imaging in the era of molecular oncology. *Nature* 2008; 452:580-589.
6. Frangioni JV. New technologies for human cancer imaging. *J Clin Oncol* 2008; 26:4012-4021.
7. Keereweer S, Kerrebijn JD, van Driel PB et al. Optical Image-guided Surgery-Where Do We Stand? *Mol Imaging Biol* 2011; 13:199-207.
8. Adams KE, Ke S, Kwon S et al. Comparison of visible and near-infrared wavelength-excitable fluorescent dyes for molecular imaging of cancer. *J Biomed Opt* 2007; 12:024017.
9. Heath CH, Deep NL, Sweeny L et al. Use of panitumumab-IRDye800 to image microscopic head and neck cancer in an orthotopic surgical model. *Ann Surg Oncol* 2012; 19:3879-3887.
10. Pomerantz RG, Grandis JR. The epidermal growth factor receptor signaling network in head and neck carcinogenesis and implications for targeted therapy. *Semin Oncol* 2004; 31:734-743.
11. Yarden Y. The EGFR family and its ligands in human cancer: signalling mechanisms and therapeutic opportunities. *Eur J Cancer* 2001; 37 Suppl 4:S3-S8.
12. Laimer K, Spizzo G, Gastl G et al. High EGFR expression predicts poor prognosis in patients with squamous cell carcinoma of the oral cavity and oropharynx: a TMA-based immunohistochemical analysis. *Oral Oncol* 2007; 43:193-198.
13. Muyldermans S, Atarhouch T, Saldanha J et al. Sequence and structure of VH domain from naturally occurring camel heavy chain immunoglobulins lacking light chains. *Protein Eng* 1994; 7:1129-1135.
14. Hamers-Casterman C, Atarhouch T, Muyldermans S et al. Naturally occurring antibodies devoid of light chains. *Nature* 1993; 363:446-448.
15. Cortez-Retamozo V, Lauwereys M, Hassanzadeh GG et al. Efficient tumor targeting by single-domain antibody fragments of camels. *Int J Cancer* 2002; 98:456-462.
16. De GE, Saerens D, Muyldermans S et al. Antibody repertoire development in camelids. *Dev Comp Immunol* 2006; 30:187-198.
17. Sabrina Oliveira, Guus A.M.S.van Dongen, Marijke Stigter-van Walsum et al. Rapid Visualization of Human Tumor Xenografts through Optical Imaging with a Near-infrared Fluorescent Anti-Epidermal Growth Factor Receptor Nanobody. *Molecular Imaging* 2011.
18. Gaikam LO, Huang L, Cavellers V et al. Comparison of the biodistribution and tumor targeting of two <sup>99m</sup>Tc-labeled anti-EGFR nanobodies in mice, using pinhole SPECT/micro-CT. *J Nucl Med* 2008; 49:788-795.
19. Yokoi T, Yamaguchi A, Odajima T et al. Establishment and characterization of a human cell line derived from a squamous cell carcinoma of the tongue. *Tumor Research* 1988;43-57.
20. Carlotti F, Bazuine M, Kekarainen T et al. Lentiviral vectors efficiently transduce quiescent mature 3T3-L1 adipocytes. *Mol Ther* 2004; 9:209-217.
21. Roovers RC, Vosjan MJ, Laeremans T et al. A biparatopic anti-EGFR nanobody efficiently inhibits solid tumour growth. *Int J Cancer* 2011; 129:2013-2024.
22. van der Linden R, de GB, Stok W et al. Induction of immune responses and molecular cloning of the heavy chain antibody repertoire of Lama glama. *J Immunol Methods* 2000; 240:185-195.
23. Dolk E, van VC, Perez JM et al. Induced refolding of a temperature denatured llama heavy-chain antibody fragment by its antigen. *Proteins* 2005; 59:555-564.
24. Oliveira S, Cohen R, Walsum MS et al. A novel method to quantify IRDye800CW fluorescent antibody probes ex vivo in tissue distribution studies. *EJNMMI Res* 2012; 2:50.

25. Roovers RC, Laeremans T, Huang L et al. Efficient inhibition of EGFR signaling and of tumour growth by antagonistic anti-EGFR Nanobodies. *Cancer Immunol Immunother* 2007; 56:303-317.
26. Troyan SL, Kianzad V, Gibbs-Strauss SL et al. The FLARE intraoperative near-infrared fluorescence imaging system: a first-in-human clinical trial in breast cancer sentinel lymph node mapping. *Ann Surg Oncol* 2009; 16:2943-2952.
27. Kim JB, Urban K, Cochran E et al. Non-invasive detection of a small number of bioluminescent cancer cells in vivo. *PLoS One* 2010; 5:e9364.
28. Mieog JS, Hutteman M, van der Vorst JR et al. Image-guided tumor resection using real-time near-infrared fluorescence in a syngeneic rat model of primary breast cancer. *Breast Cancer Res Treat* 2010.
29. van Dam GM, Crane LM, Themelis G et al. Intraoperative tumor-specific fluorescence imaging in ovarian cancer by folate receptor-alpha targeting: first in-human results. *Nat Med* 2011; Sep 18;17(10):1315-9.
30. Keereweer S, Sterenborg HJ, Kerrebijn JD et al. Image-guided surgery in head and neck cancer: current practice and future directions of optical imaging. *Head Neck* 2012; 34:120-126.
31. Grandis JR, Tweardy DJ. Elevated levels of transforming growth factor alpha and epidermal growth factor receptor messenger RNA are early markers of carcinogenesis in head and neck cancer. *Cancer Res* 1993; 53:3579-3584.
32. Keereweer S, Kerrebijn JD, Mol IM et al. Optical imaging of oral squamous cell carcinoma and cervical lymph node metastasis. *Head Neck* 2012; 34:1002-1008.
33. Gleysteen JP, Duncan RD, Magnuson JS et al. Fluorescently labeled cetuximab to evaluate head and neck cancer response to treatment. *Cancer Biol Ther* 2007; 6:1181-1185.
34. Gioux S, Choi HS, Frangioni JV. Image-guided surgery using invisible near-infrared light: fundamentals of clinical translation. *Mol Imaging* 2010; 9:237-255.
35. Mieog JS, Troyan SL, Hutteman M et al. Toward optimization of imaging system and lymphatic tracer for near-infrared fluorescent sentinel lymph node mapping in breast cancer. *Ann Surg Oncol* 2011; 18:2483-2491.
36. Heukers R, Vermeulen JF, Fereidouni F et al. Endocytosis of EGFR requires its kinase activity and N-terminal transmembrane dimerization motif. *J Cell Sci* 2013; 126:4900-4912.
37. Keereweer S, Mol IM, Kerrebijn JD et al. Targeting integrins and enhanced permeability and retention (EPR) effect for optical imaging of oral cancer. *J Surg Oncol* 2012; 105:714-718.
38. Leemans CR, Tiwari R, Nauta JJ et al. Regional lymph node involvement and its significance in the development of distant metastases in head and neck carcinoma. *Cancer* 1993; 71:452-456.
39. Layland MK, Sessions DG, Lenox J. The influence of lymph node metastasis in the treatment of squamous cell carcinoma of the oral cavity, oropharynx, larynx, and hypopharynx: N0 versus N+. *Laryngoscope* 2005; 115:629-639.
40. van der Vorst JR, Schaafsma BE, Verbeek FP et al. Near-infrared fluorescence sentinel lymph node mapping of the oral cavity in head and neck cancer patients. *Oral Oncol* 2012.



